Delayed induction of type I and III interferons and nasal epithelial cell permissiveness to SARS-CoV-2

Nasal interferon responses to SARS-CoV-2

Authors

Catherine F Hatton[1a], Rachel A Botting[2a], Maria Emilia Dueñas[2a], Iram J Haq[1,3a], Bernard Verdon[2a], Benjamin J Thompson[1], Jarmila Stremenova Spegarova[1], Florian Gothe[1,4], Emily Stephenson[2], Aaron I Gardner[1], Sandra Murphy[2], Jonathan Scott[1], James P Garnett[1], Sean Carrie[5], Rafiqul Hussain[6], Jonathan Coxhead[6], Tracey Davey[7], A John Simpson[1], Muzlifah Haniffa[2,8,9,10], Sophie Hambleton[1,11], Malcolm Brodlie[1,3b], Chris Ward[1b], Matthias Trost[2b], Gary Reynolds[2b], Christopher J A Duncan[1,12 b]*

[a] equal contribution

[b] equal contribution

* corresponding author: christopher.duncan@ncl.ac.uk

Affiliations

1. Translational and Clinical Research Institute, Faculty of Medical Sciences, Newcastle University, Newcastle upon Tyne, UK.

2. Biosciences Institute, Newcastle University, Newcastle upon Tyne, UK.

3. Paediatric Respiratory Medicine, Great North Children's Hospital, Newcastle upon Tyne Hospitals NHS Foundation Trust, Newcastle upon Tyne, UK.

4. Department of Pediatrics, Dr. von Hauner Children's Hospital, University Hospital, Ludwig-Maximilians-Universität Munich, Munich, Germany.

5. Population Health Sciences Institute, Newcastle University, Newcastle upon Tyne, UK.

6. Genomics Core Facility, Biosciences Institute, Newcastle University, Newcastle upon Tyne, UK.

7. Electron Microscopy Research Services, Newcastle University, Newcastle upon Tyne, UK.

8. NIHR Newcastle Biomedical Research Centre, Newcastle Hospitals NHS Foundation Trust, Newcastle upon Tyne, UK

9. Department of Dermatology, Newcastle Hospitals NHS Foundation Trust, Newcastle upon Tyne, UK

10. Wellcome Sanger Institute, Wellcome Genome Campus, Cambridge, UK

11. Great North Children's Hospital, Newcastle upon Tyne Hospitals NHS Foundation Trust, UK.

12. Department of Infection and Tropical Medicine, Newcastle upon Tyne Hospitals NHS Foundation Trust, UK.

Abstract

The nasal epithelium is a plausible entry point for SARS-CoV-2, a site of pathogenesis and transmission, and may initiate the host response to SARS-CoV-2. Antiviral interferon responses are critical to outcome of SARS-CoV-2. Yet little is known about the interaction between SARS-CoV-2 and innate immunity in this tissue. Here we applied single-cell RNA sequencing and proteomics to a primary cell model of human primary nasal epithelium differentiated at air-liquid interface. SARS-CoV-2 demonstrated widespread tropism for nasal epithelial cell types. The host response was dominated by type I and III IFNs and interferon-stimulated gene products. Nevertheless, this response was notably delayed in onset compared to viral gene expression, and thus failed to impact substantially on SARS-CoV-2 replication. However, when provided prior to infection, recombinant IFNβ or IFNλ1 induced an efficient antiviral state that potently restricted SARS-CoV-2 viral replication, preserving epithelial barrier integrity. These data suggest nasal delivery of recombinant IFNs to be a potential chemoprophylactic strategy.

49 **INTRODUCTION**

50 SARS-CoV-2 is an emergent betacoronavirus responsible for coronavirus disease-19 (COVID-19)[1]. Since
51 its identification in late 2019, global pandemic transmission of SARS-CoV-2 has resulted in over 105
52 million infections and approximately 2.9 million deaths. SARS-CoV-2 infects target cells via the entry
53 receptor ACE2[2] leading to a spectrum of clinical outcomes, ranging from asymptomatic infection to
54 death[3]. Although multiple host factors (e.g. age, sex, obesity) contribute to adverse clinical outcome[4],
55 the immune response also plays a decisive role, evidenced by the therapeutic benefit of
56 immunomodulatory agents including corticosteroids[5]. Yet much remains to be understood about the
57 immunopathogenesis of COVID-19. Identification of the cells hosting viral entry and characterisation
58 of their response to infection is essential to understanding pathogenesis and improving therapy.

59 The nasal epithelium is believed to be a key entry point of SARS-CoV-2. Nasal epithelial tropism and
60 efficient viral shedding from the nasopharynx apparently contributes to the high transmissibility of
61 SARS-CoV-2[6], as well as to pathologic features such as anosmia[7]. As an early viral target cell, nasal
62 epithelial cells may also set the tone for the systemic immune response, potentially influencing disease
63 outcome[8]. These factors emphasise the need to study host-virus interaction in human nasal cells. *Ex*
64 *vivo* single-cell transcriptomic studies indicate that ciliated and/or goblet cells in the nasal mucosa
65 express *ACE2* and *TMPRSS2,* implicating them as probable SARS-CoV-2 target cells[9,10]. This has been
66 confirmed by *in vitro* and *in vivo* studies demonstrating SARS-CoV-2 infection of human nasal epithelial
67 cells[11-13]. Single-cell studies also revealed that nasal cells exhibit basal expression of an antiviral
68 expression programme, characterised by induction of several interferon-stimulated genes (ISGs),
69 suggesting that they may be primed to respond to viral infection[9]. Interestingly, *ACE2* is also regulated
70 by interferons (IFNs) [10,14], implying a complex relationship between IFN signalling and tropism. Type I
71 and type III IFN (IFN-I/III) systems play a critical role in human antiviral innate immunity[15] and have
72 been recently implicated in defence against SARS-CoV-2: susceptibility to severe or life-threatening
73 COVID-19 is associated with deleterious variants in *IFNAR* genes[16,17] and IFN-I blocking
74 autoantibodies[18]. *In vitro*, SARS-CoV-2 appears sensitive to the antiviral properties of IFN-I, at least in

75 cell lines[19,20], and this activity extends to *in vivo* model systems[8]. These findings motivate studies to
76 improve understanding of the interaction between SARS-CoV-2 and the IFN-I system in primary human
77 target cells, providing impetus to clinical trials of recombinant IFNs in treatment or prophylaxis of
78 COVID-19[21].
79 Organotypic cultures of primary human nasal epithelium differentiated at air-liquid interface (ALI) are
80 a translationally-relevant primary cell model for studies of SARS-CoV-2 host-virus interaction[11], with
81 considerable potential to accelerate our understanding of pathogenesis. A small number of studies
82 using this model demonstrate that SARS-CoV-2 replicates efficiently in human nasal cells[11-13], yet
83 important questions concerning cellular tropism and their innate immune response remain
84 unresolved. Hou and colleagues report that only ciliated cells were permissive to SARS-CoV-2, despite
85 expression of ACE2 and TMPRSS2 by all cell types[12]. They hypothesised that post-entry factors, such
86 as innate immunity, might govern tropism. By contrast, Pizzorno and colleagues reported infection in
87 all major cell types (ciliated, secretory and basal cells)[13], consistent with prior indications from single
88 cell RNA sequencing (scRNA-seq) data and studies in lower airway models[22,23]. While an IFN response
89 to SARS-CoV-2 can be detected in nasal cells[11,13], in apparent contrast to bronchial or alveolar
90 epithelial cells[24-26], the kinetics of induction and the antiviral function of IFNs in nasal epithelium has
91 not been systematically characterised.
92 Here we employed a comprehensive range of techniques, including scRNA-seq and proteomics, in
93 primary human nasal ALI cultures to define: (i) cellular tropism; (ii) the innate immune response to
94 SARS-CoV-2; and (iii) the antiviral activity of IFN-I/III. We observed broad cellular tropism of SARS-CoV-
95 2 for nasal epithelial cells, although ciliated cells were the most permissive. Nasal cells mounted a
96 delayed IFN response that failed to exert control over viral replication. However, SARS-CoV-2
97 remained highly sensitive to IFN-restriction if exogenous IFN-I/III was applied prior to infection. These
98 data enrich our understanding of the interaction of SARS-CoV-2 and the human IFN system at the
99 earliest point of infection, with immediate therapeutic implications.
100

101 **RESULTS**

102 **SARS-CoV-2 robustly infects primary differentiated nasal epithelial cultures**

103 Primary nasal epithelial cultures were established from cryopreserved stocks from six adult donors,
104 obtained prior to the SARS-CoV-2 pandemic. Cells were expanded, differentiated and then matured
105 at ALI for 28 days, according to an established protocol[27]. We first sought to address their suitability
106 as a model of SARS-CoV-2 infection. Visualisation of scRNA-seq data from two representative donors
107 discerned five major populations of cells (Fig. 1A). These were ciliated, secretory and basal cells,
108 alongside two rarer populations of FOXN4+ cells and ionocytes. Cells expressed characteristic markers
109 (Fig. 1B) and corresponded broadly to *ex vivo* single-cell data from nasal biopsies[9,10]. Immunostaining
110 verified the presence of major cell types in these cultures - including acetylated alpha-tubulin-positive
111 (AAT) ciliated cells, mucin 5B-positive (MUC5B) secretory cells, and tumour protein 63-positive (TP63)
112 basal cells (Fig. 1C) - with ciliated cells being the most frequent cell population. Consistent with
113 published scRNA-seq data, mRNA for key SARS-CoV-2 entry receptors, *ACE2* and *TMPRSS2*, was
114 expressed, albeit at relatively low levels, alongside other genes implicated in possible alternate modes
115 of SARS-CoV-2 entry such as *FURIN* and *CTSL* (Fig. S1)[28]. Robust expression of ACE2 and TMPRSS2 at
116 the protein level was confirmed by immunoblotting of whole-cell lysates prepared from mature ALI
117 cultures (Fig. 1D). To establish their permissiveness to infection, nasal ALI cultures were inoculated at
118 the apical surface with a clinical SARS-CoV-2 isolate (England/2/20) at an approximate multiplicity of
119 infection (MOI) 0.1 - consistent with other studies (0.1-0.5)[11-13] - and monitored for infection over the
120 next 72 h. Expression of SARS-CoV-2 *nucleocapsid (N)* gene and spike (S) protein increased significantly
121 over time, indicative of viral replication (Fig. 1E-F). This was accompanied by the release of infectious
122 viral particles, as determined by plaque assay of apical washes on Vero E6 cells, confirming productive
123 infection (Fig. 1G). SARS-CoV-2 replication was accompanied by a progressive decline in epithelial
124 barrier integrity starting from 48 hours post-infection (hpi), reflecting virus-induced epithelial
125 dysfunction (Fig. 1H). These data established the suitability of the human nasal ALI model for
126 modelling SARS-CoV-2 infection.

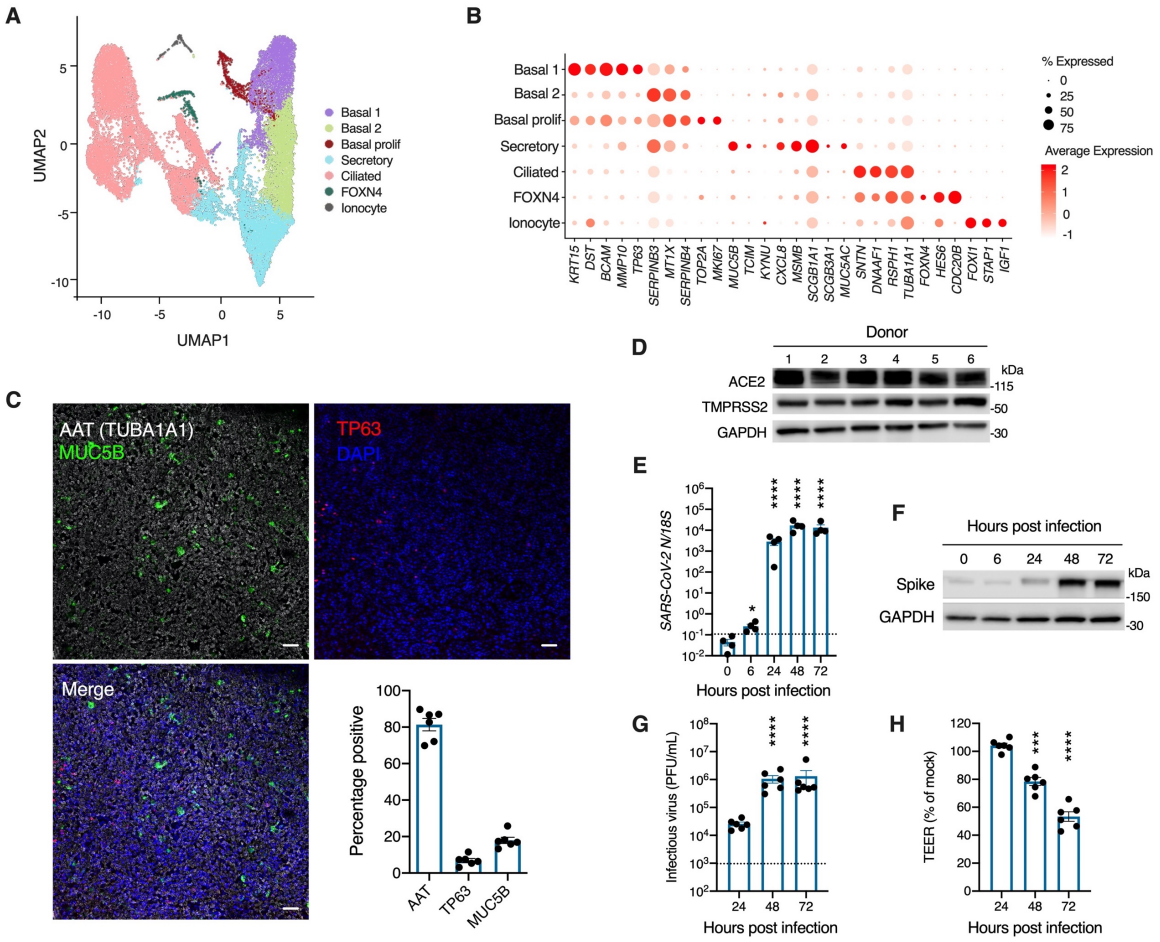

Figure 1. Robust SARS-CoV-2 infection in a primary differentiated nasal epithelial ALI culture model. (A) UMAP visualisation of scRNA-seq data in nasal ALI cultures revealed five major cell types. (B) Expression of key markers distinguishing cell types. (C) Immunofluorescence analysis of secretory (MUC5B), ciliated (AAT) and basal (TP63) cells in nasal ALI cultures (representative images from n=6 donors, scale bar = 20 μm), with frequency of cell type summarised in the bar plot. (D) Immunoblot demonstrating ACE2 and TMPRSS2 expression by each donor, representative of n=3 experiments. (E) RT-PCR analysis of SARS-CoV-2 nucleocapsid (*N*) gene expression in whole-cell lysate (WCL) (repeat experiments in n=6 donors). (F) Immunoblot of SARS-CoV-2 spike (S) protein expression in WCL (representative of repeat experiments in n=4 donors). (G) Production of infectious viral particles determined by plaque assay of apical washings (repeat experiments in n=6 donors). Dotted line represents lower limit of detection. (G) Transepithelial resistance (TEER) measurements upon infection (expressed as % of mock-infected wells, mean of repeat experiments in n=6 donors). Mean

140 ± SEM. * P < 0.05, **** P < 0.001 ANOVA with Dunnett's post-test correction, comparing to 0h (E) or
141 24h (G-H). MUC5B, mucin 5B; AAT, acetylated alpha tubulin; TP63, tumour protein 63.
142
143
144 **Evidence of broad cellular tropism of SARS-CoV-2**
145 To revisit the question of whether individual cell types are more or less permissive to SARS-CoV-2[12,13],
146 we first examined viral gene expression by scRNA-seq analysis at 24 hpi, selected to represent an early
147 stage in the progress of infection. Of the viral transcripts, the *N* gene was most abundantly expressed
148 (Fig. 2A). While all cell types expressed viral transcripts, there were notable differences both in the
149 proportion of cells infected, and the relative abundance of different viral transcripts within these cells.
150 A greater proportion of ciliated and secretory cells expressed viral transcripts compared to basal cells
151 (Fig. 2B). However basal cells are located away from the apical surface; physical inaccessibility to
152 apically-applied virus at this timepoint might at least partially account for this observation. To
153 investigate tropism further, we undertook immunofluorescence analysis of viral spike (S) protein
154 expression at 48 hpi. This analysis revealed broadly similar proportions of ciliated, secretory and basal
155 cells expressing S protein. However, the mean pixel intensity of S protein was significantly greater in
156 ciliated cells (Fig. 2C-D). To corroborate these findings, we undertook analysis of intracellular virion-
157 like structures (VLSs) at 48 hpi by transmission electron microscopy (TEM, Fig 2E), focusing on ciliated
158 and secretory cells. Intracellular VLSs were observed in both ciliated and secretory cells,
159 predominantly towards the apical surface (Fig. 2E). Consistent with immunofluorescence analysis of S
160 protein intensity, there was a significant increase in the number of VLSs per cell in ciliated compared
161 with secretory cells (Fig. 2E). Collectively, these data suggested that the virus is capable of entering,
162 and replicating in, all major nasal cell types.
163

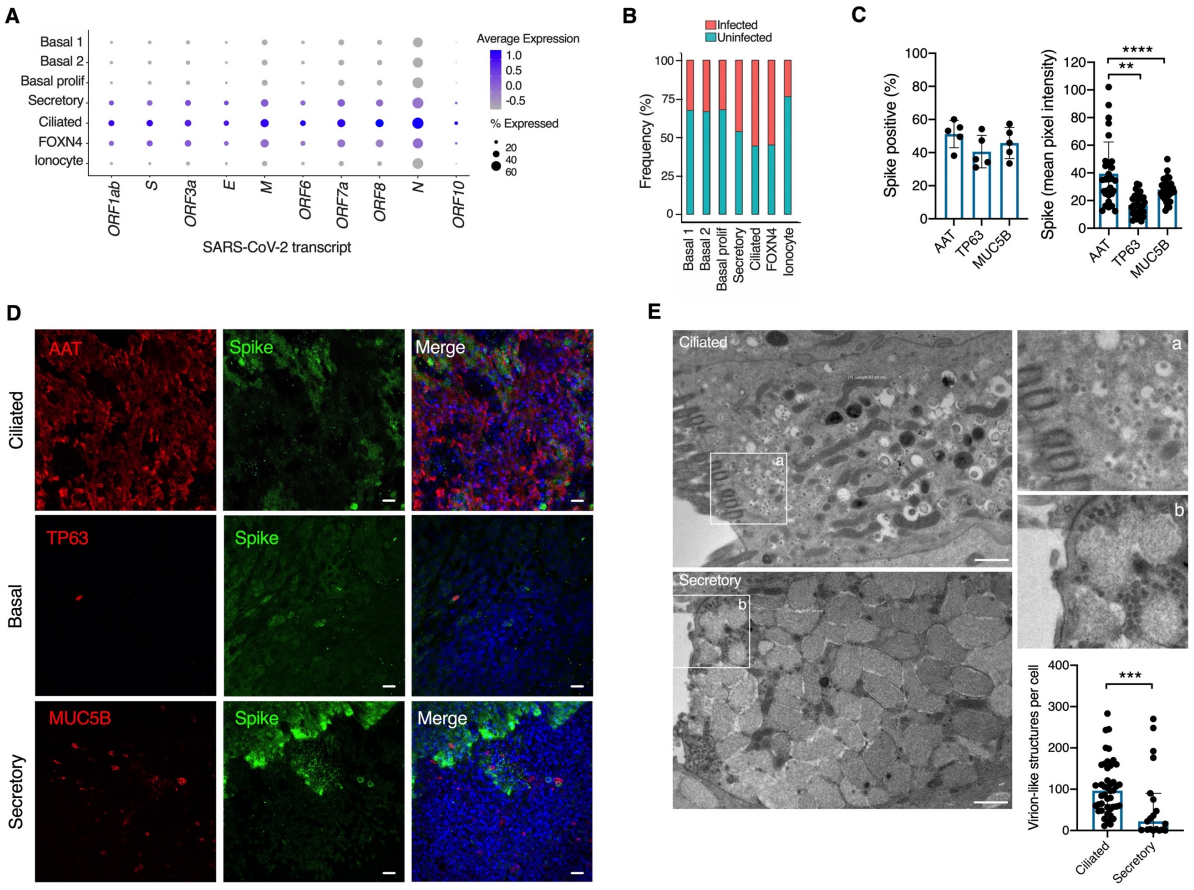

Figure 2. Broad tropism of SARS-CoV-2 for nasal cells. (A) Dot plot of scRNA-seq data showing magnitude (colour) and proportion (size) of cell types expressing viral transcripts. (B) Relative proportion of infected cell types based on expression of viral spike (*S)* gene. (C) Quantification of cell-type specific expression of viral S protein and S intensity at 48 hpi (repeat experiments in n=5 donors). (D) Representative images of viral S protein expression in ciliated (AAT), secretory (MUC5B) and basal cells (TP63) shown in (C). Scale bars = 10 µm. (E) Transmission electron micrograph (TEM) analysis of SARS-CoV-2 infected ciliated and secretory cells at 48 hpi, with quantification of virion-like structures in the bar plot. Inserts (a) and (b) display VLSs in ciliated and secretory cells respectively. Scale bars = 1 µm. Mean ± SEM ** P < 0.01, *** P < 0.001, **** P < 0.0001, ANOVA with Dunnett's post-test correction (C) or t-test (E). E = envelope; M = matrix; N = nucleocapsid; S = spike.

Characterisation of nasal cell responses to SARS-CoV-2

178 Published *ex vivo* single-cell transcriptomic analyses report that nasal cells exhibit the basal expression
179 of an innate antiviral programme, in the absence of viral infection, characterised by several ISGs[9]. This
180 suggests that nasal epithelial cells may adopt a constitutive antiviral state. It was also hypothesised
181 that cellular innate immunity might influence nasal cell tropism of SARS-CoV-2[12].
182 In epithelial cells, ISGs are predominantly regulated by paracrine signalling mediated by IFN-I/IIIs. IFN-
183 I/IIIs are produced by virally infected cells, downstream of pattern-recognition receptor (PRR)
184 signalling, alerting their neighbours to viral infection. Responding cells adopt an antiviral state as a
185 consequence of the expression of hundreds of antiviral ISGs[29]. Receptors for both IFN-I (IFNAR) and
186 IFN-III (IFNLR) are expressed by epithelial cells. Ligand binding to these receptors activates a shared
187 JAK-STAT signalling pathway, culminating in ISG expression[15,29]. However, ISGs can also be regulated
188 by IFN-independent mechanisms. These include the direct action of constitutively expressed
189 transcription factors such as IRF3, activated downstream of PRRs[29], or by constitutive ISG expression
190 - a strategy employed by stem cells for antiviral defence[30].
191 We examined scRNA-seq data to characterise the innate antiviral response of nasal cells, both at
192 baseline and in response to SARS-CoV-2 infection at 24 hpi. For this analysis we distinguished cells in
193 three experimental conditions: unexposed (mock-infected); SARS-CoV-2-exposed but uninfected
194 (these cells would theoretically be exposed to IFNs and other paracrine signals, but not infected); and
195 SARS-CoV-2-infected (as defined by expression of *S* transcripts). At baseline, expression of a composite
196 ISG signature (Fig. 3A) and individual ISGs (Fig. 3B) was observed in unexposed cell types, consistent
197 with *ex vivo* scRNA-seq findings[9]. Considering that viral infection occurred in all cell types, these data
198 imply that relative differences in the basal ISG expression programmes did not substantially impact on
199 SARS-CoV-2 permissiveness, at least under the infection conditions studied here. We next considered
200 the involvement of paracrine IFNs. In SARS-CoV-2 infected cells, but not their uninfected neighbours,
201 we observed an enrichment of the ISG signature (Fig. 3A-B). This finding is more suggestive of direct
202 induction of ISGs in infected cells, rather than paracrine IFN-I/III signalling, at least at this timepoint.
203 Consistent with this, we observed expression of IFN-I (*IFNB, IFNK, IFNA5)* and IFN-III (*IFNL1-3)* in only

204 a small minority (0.1%) of infected ciliated cells, and very low levels in other nasal cell types (Fig. 3C).
205 Considering that over 50% of ciliated cells expressed viral transcripts at this timepoint, these data
206 suggest that SARS-CoV-2 efficiently avoided IFN induction in the vast majority of infected epithelial
207 cells, consistent with data in non-nasal airway epithelial cells[25,26]. A range of other chemokines and
208 cytokines were induced by infected epithelial cells, indicating the preserved capacity to detect viral
209 infection (Fig. S2).
210

211

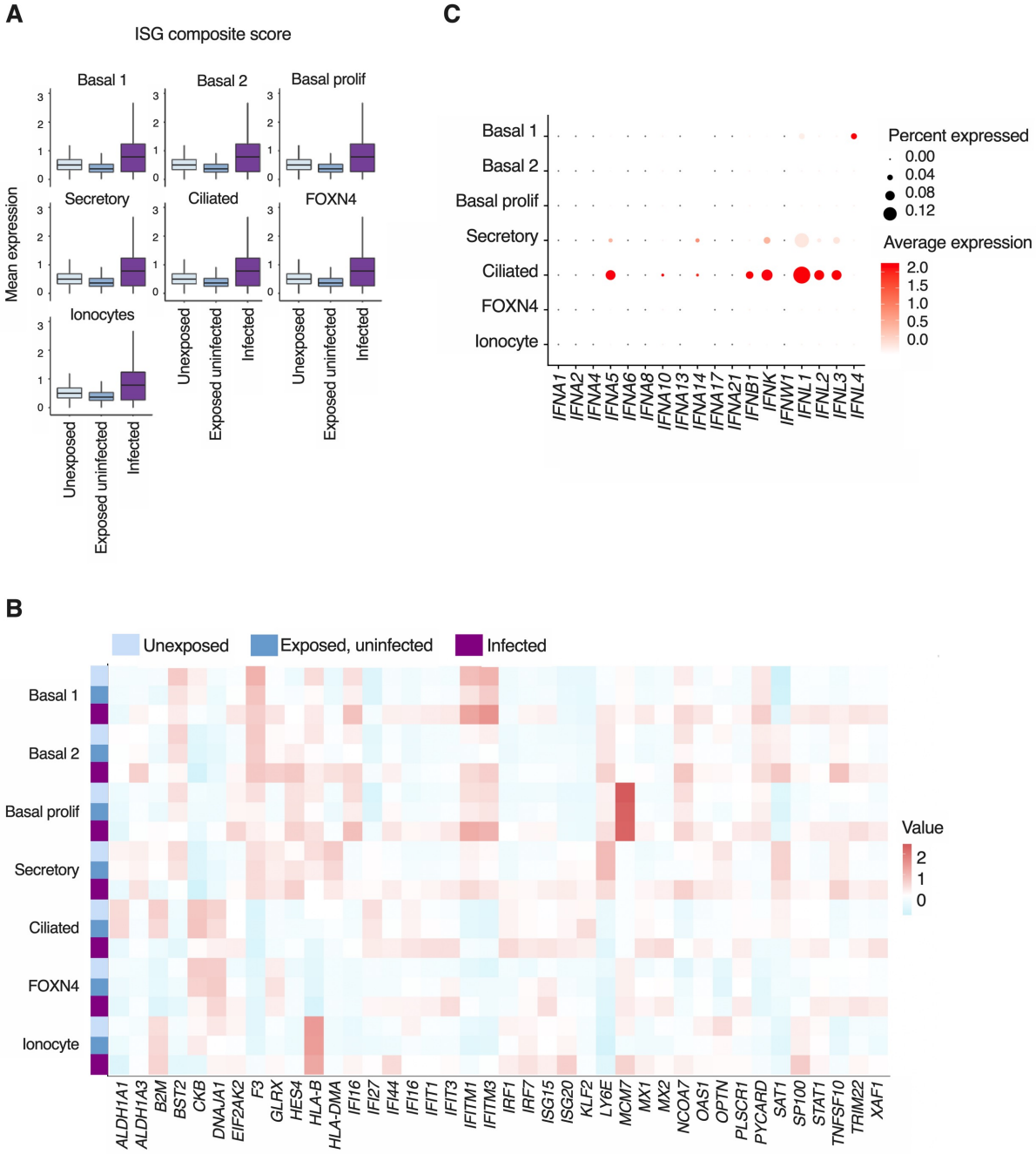

212

213 **Figure 3. Characterisation of innate IFN responses in nasal cells.** (A) Average expression of interferon-

214 stimulated gene (ISG) composite score signature genes in SARS-CoV-2 unexposed (light blue), SARS-

215 CoV-2 exposed but uninfected (blue), and SARS-CoV-2 infected (purple) cell types at 24 hpi. Boxes

216 represent the median value +/- 1.58*IQR/√(n) and whiskers represent 1.5*IQR. Outliers outside this

217 range were trimmed. Differences between infected and other cell types were significant by FDR-

218 adjusted ANOVA at $P < 0.001$. (B) Matrix plot demonstrating expression (colour) of individual ISGs

219 making up composite score in (A). (C) Dot plot of individual differentially-expressed IFNs by cell type
220 (normalised expression compared to uninfected cells, with colour representing mean expression and
221 size of the dot representing the proportion of cells expressing each gene).
222
223
224 **Kinetics of innate IFN-I/IFN-IIIs response to SARS-CoV-2**
225 To investigate the kinetics of the IFN-I/III response, expression of IFN-I (*IFNA1* and *IFNB*) and IFN-III
226 (*IFNL1*) was examined by RT-PCR at 6, 24, 48 and 72 hpi (Fig. 4A). Induction of *IFNL1* and *IFNB* was low
227 at 24 hpi, consistent with scRNA-seq findings, but increased significantly by 48 and 72 hpi. *IFNA1* was
228 not induced, as observed in our scRNA-seq data. Compared to the timing of initiation of viral gene
229 expression - which was detectable at 6 hpi and approached its maximum level by 24 hpi (Fig. 1E) - the
230 induction of IFNs appeared delayed, as suggested by previous studies[11,13]. Infection was accompanied
231 by progressive upregulation of proinflammatory cytokines such as *IL1B, IL6* and *TNF*, consistent with
232 initiation of a local inflammatory response (Fig. 4B). To confirm that the attenuated production of
233 *IFNL1* and *IFNB* at early times was not dependent on MOI or due to an intrinsic defect of these cells,
234 infections were repeated at high MOI (~ 2). Infections at high MOI have been previously reported to
235 enhance the relatively inefficient IFN-I induction in response to SARS-CoV-2[25]. A preparation of Sendai
236 virus (SeV) - containing a high proportion of immunostimulatory defective viral genomes (DVGs) - was
237 used as a positive control. At 6 hpi, a time point at which *IFNB* and *IFNL1* were robustly induced by
238 SeV DVGs, there was no response to SARS-CoV-2 infection at high MOI (Fig. 4C), despite SARS-CoV-2
239 gene expression (Fig. 4C). Thus SARS-CoV-2 appears to efficiently evade PRR detection in nasal
240 epithelial cells. To look for evidence of a paracrine response to IFN-I/III, we undertook analysis of
241 expression of the ISGs *RSAD2* and *USP18* by RT-PCR and immunoblotting (Fig. 4D-E). This analysis
242 revealed an increase in ISG expression at later times (48-72 hpi), corresponding to the expression of
243 *IFNB*/*IFNL1*. This association is suggestive (although not causal evidence) of paracrine IFN-I/III

244 signalling. Collectively, these results indicate that nasal epithelial cells are capable of expressing IFN-

245 I/IIIs during SARS-CoV-2 infection, but that the response is delayed relative to viral replication.

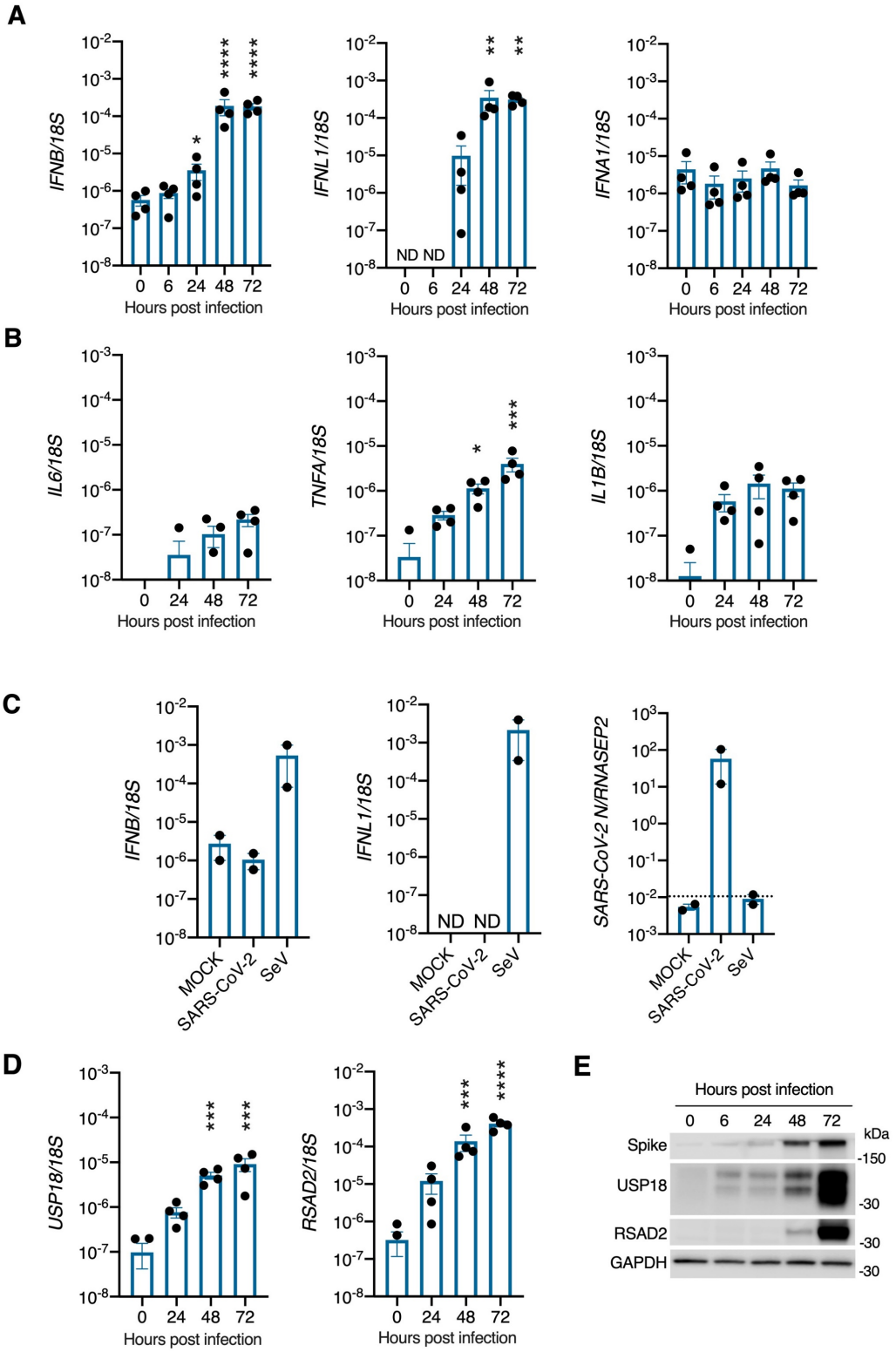

246

247 **Figure 4. Delayed induction of IFN-I/III signalling in SARS-CoV-2-infected nasal ALI cultures.** (A) RT-

248 PCR analysis of expression of (A) *IFNB*, *IFNL1* and *IFNA1* and (B) *IL6*, *TNFA* and *IL1B* expression in whole-

249 cell lysates (repeat experiments in n=4 donors). (C) RT-PCR analysis of *IFNB*, *IFNL1* and SARS-CoV-2 *N*
250 gene expression in nasal ALI cultures exposed to SARS-CoV-2 (MOI = 2) or a DVG-rich stock of Sendai
251 virus (SeV) for 6 h (repeat experiments in n=2 donors). (D) RT-PCR and (E) immunoblot analysis of
252 *USP18* and *RSAD2* expression in whole-cell lysates (repeat experiments in n=4 donors). ND, Not
253 detected. Mean ± SEM * $P < 0.05$, ** $P < 0.01$, *** $P < 0.001$ **** $P < 0.0001$, ANOVA with Dunnett's
254 post-test correction compared to 0h (A [*IFNB*]) or 24h (A [*IFNL1*], B, D).
255
256
257 **IFN-signalling dominates the nasal host response to SARS-CoV-2 at the protein level**
258 To validate and extend these findings, we undertook an unbiased assessment of the host response to
259 SARS-CoV-2 infection by proteomics analysis. Whole-cell lysates were prepared from SARS-CoV-2 and
260 mock-infected nasal ALI cultures from six donors at 72 hpi. Lysates were analysed by quantitative mass
261 spectrometry (Supplementary Dataset S1, quality control data in Fig. S3). Overall, this analysis
262 detected the differential expression (DE) of 180 proteins including viral proteins such as S, M, N,
263 ORF1AB, ORF3A and ORF8 (Fig. 5A). The most highly increased host protein was Sorting Nexin 33
264 (SNX33), an endosomal protein that has not yet been implicated in the life cycle of SARS-CoV-2.
265 Infected and uninfected cells clustered together by principal component analysis (Fig. 5B). Inspection
266 of the DE proteins confirmed a robust host innate immune response, dominated by ISG products (Fig.
267 5A). Functional annotation revealed an enrichment of antiviral response and especially IFN-I signalling
268 pathways (Fig. 5C, Table S1). These data are consistent with our earlier findings and contrary to prior
269 reports in cell lines or human bronchial/tracheal epithelial cultures, where a robust endogenous IFN-
270 I/III response to SARS-CoV-2 was not detected[24-26]. Key ISG proteins identified included IFITM1-3 and
271 the OAS cluster (OAS1-3), the latter associated with genetic susceptibility to severe COVID-19[17] (Fig.
272 5C). Significantly downregulated pathways were also identified, including TRIF-dependent toll-like
273 receptor signalling, as well as RNA polymerase II transcription and endosomal transport (Table S2).
274 This implied viral subversion of critical host functions, including host gene transcription, protein

trafficking and viral sensing. Proteins involved in the maintenance of epithelial tight junctions were also downregulated, consistent with the loss of barrier integrity observed in earlier experiments (Fig. 1H).

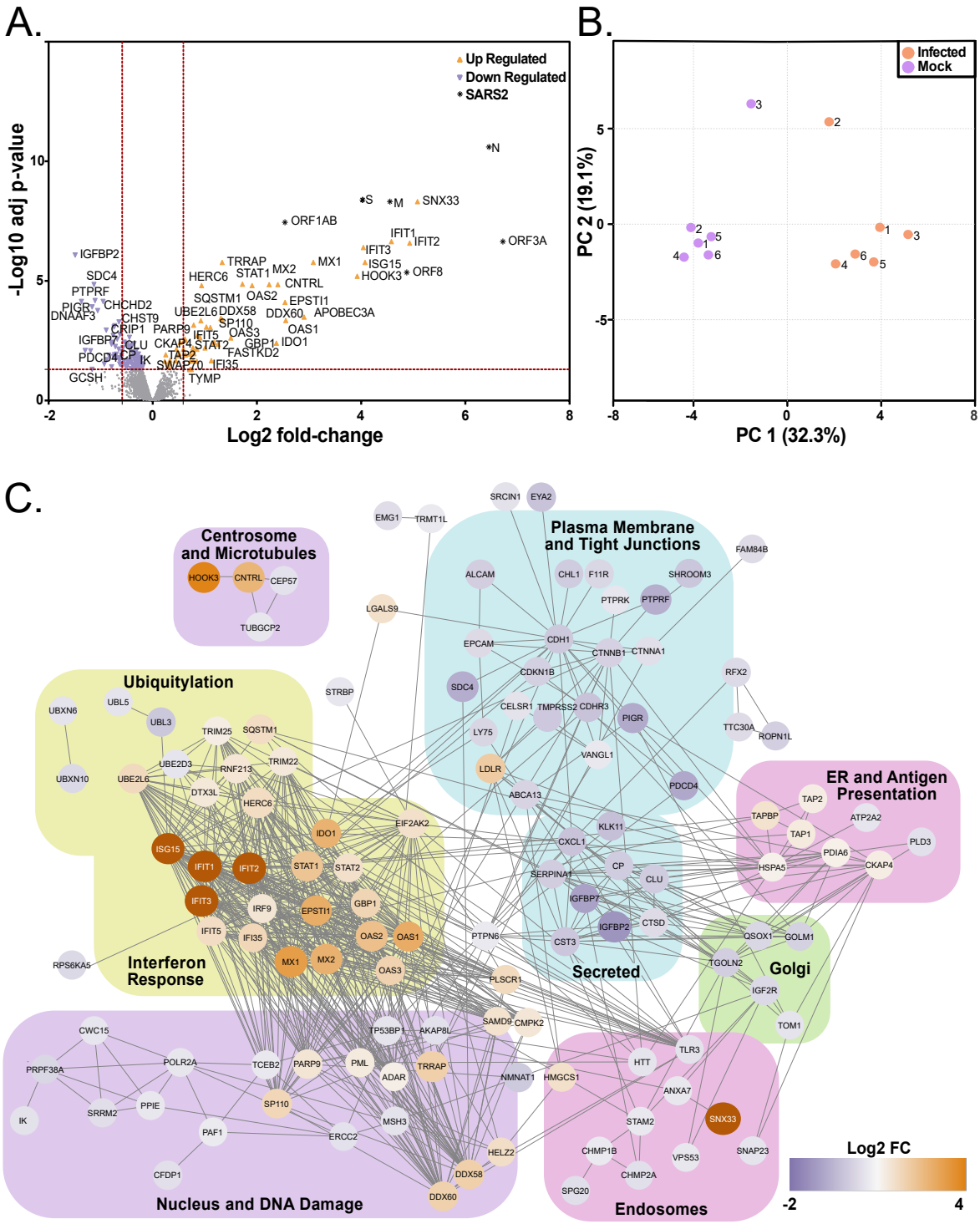

280 **Figure 5. An ISG response dominates the proteome of SARS-CoV-2 infected nasal ALI cultures**.
281 Differential proteomic profiling of SARS-CoV-2-infected nasal ALI cultures. Mass spectrometry-based
282 proteomics was carried out on whole-cell lysates prepared at 72 hpi (n=6 donors per condition). (A)
283 Volcano plot illustrating 180 differentially expressed proteins with increased (orange points) and
284 decreased (purple points) expression in infected as compared to mock samples. Dotted red lines
285 indicate those proteins with a fold change of < 1.5 and adjusted p values <0.05. (B) Principal
286 component analysis of the whole proteome data set. (C) Functional annotation network of
287 differentially expressed proteins.
288
289
290 **Antiviral activity of IFN-I/III towards SARS-CoV-2 infection**
291 Given the prominence of the IFN-I/III response in the proteome of SARS-CoV-2-infected cells, a key
292 question was whether the IFN-I/III response had any impact on SARS-CoV-2 replication. To address
293 this question, nasal ALI cultures were treated with the JAK inhibitor ruxolitinib (RUX). RUX antagonises
294 signalling downstream of IFNAR and IFNLR, owing to the involvement of JAK1 in both signalling
295 pathways. We reasoned that blocking paracrine IFN-I/III signalling would reveal its impact, if any, on
296 SARS-CoV-2 replication. Cells were treated with 10 µM RUX (a dose optimised in prior experiments[31])
297 or vehicle control (DMSO) in the basal medium for 24 hours prior to infection. Nasal cultures were
298 infected at the apical surface (MOI ~ 0.01) and inhibitors were refreshed every 24h. At 48 hpi, lysates
299 were prepared and analysed by immunoblot. RUX treatment abolished expression of RSAD2 and
300 USP18 in response to SARS-CoV-2 infection (Fig. 6A), indicating that induction of ISG protein products
301 at this timepoint was largely dependent on paracrine IFN-I/III signalling, as previously suggested (Fig.
302 4D). However, viral S protein expression was not enhanced by RUX treatment (Fig. 6A), nor was release
303 of infectious virus, as measured by plaque assay (Fig. 6B). These data suggested that the endogenous
304 IFN-I/III response failed to impact SARS-CoV-2 replication up to 48 hpi, at least at the MOI tested.
305 These data provided further evidence that SARS-CoV-2 triggers an endogenous paracrine IFN-I/III

306 response in nasal cells, but showed that this response was insufficient to contain SARS-CoV-2
307 replication.
308 An important follow-up question was whether nasal cells could mount an antiviral state to SARS-CoV-
309 2, providing IFN-I/III was delivered in a timely fashion. To address this, nasal ALI cultures were pre-
310 treated with exogenous IFNβ or IFNλ1 for 16h to induce an antiviral state, subsequently infected with
311 SARS-CoV-2 at MOI 0.01, and examined at 48 hpi. Analysis of infection by immunoblotting of whole-
312 cell lysates for spike (S) protein expression or plaque assay of apical washes demonstrated a significant
313 reduction in infection with either IFNβ or IFNλ1 pre-treatment (Fig. 6C-D). This was accompanied by
314 robust induction of antiviral ISG products (Fig. 6C), and preservation of barrier integrity (Fig. S4). It is
315 worth noting that the ISG expression induced in response to recombinant IFN-I/III was substantially
316 greater than that induced by SARS-CoV-2 infection (i.e. endogenous IFN-I/III production, Fig. 6C). Thus
317 exogenous IFN-I/III was capable of inducing in the nasal epithelium an antiviral state that potently
318 inhibited SARS-CoV-2 infection, providing it was delivered (a) prior to infection, and (b) at sufficient
319 concentration. This IFN-sensitivity of SARS-CoV-2 contrasts with the relative resistance of SARS-CoV[19].
320 These data suggest that mucosal delivery of IFNβ is a potential therapeutic strategy for SARS-CoV-2.
321 In clinical practice, IFNs are unlikely to be used prior to infection, unless this is part of a prophylactic
322 regimen. To determine the effectiveness of exogenously applied IFN-I once SARS-CoV-2 infection is
323 underway, cells were treated with IFNβ at 6 or 24 hpi. In this experiment, IFNβ treatment at 6 hpi
324 continued to impact on SARS-CoV-2 infection, whereas addition after 24 hpi had no effect (Fig. 6E-F).
325 Interestingly, ISG induction was still observed in response to IFNβ treatment at 24 hpi, albeit at
326 reduced magnitude (Fig. 6E). These data suggest that SARS-CoV-2 impairs, but does not abolish, JAK-
327 STAT signalling in infected cells, implying that recombinant IFNs may have a therapeutic role in
328 established SARS-CoV-2 infection, as recently shown in animal models[8] and in early phase clinical
329 trials[32].
330

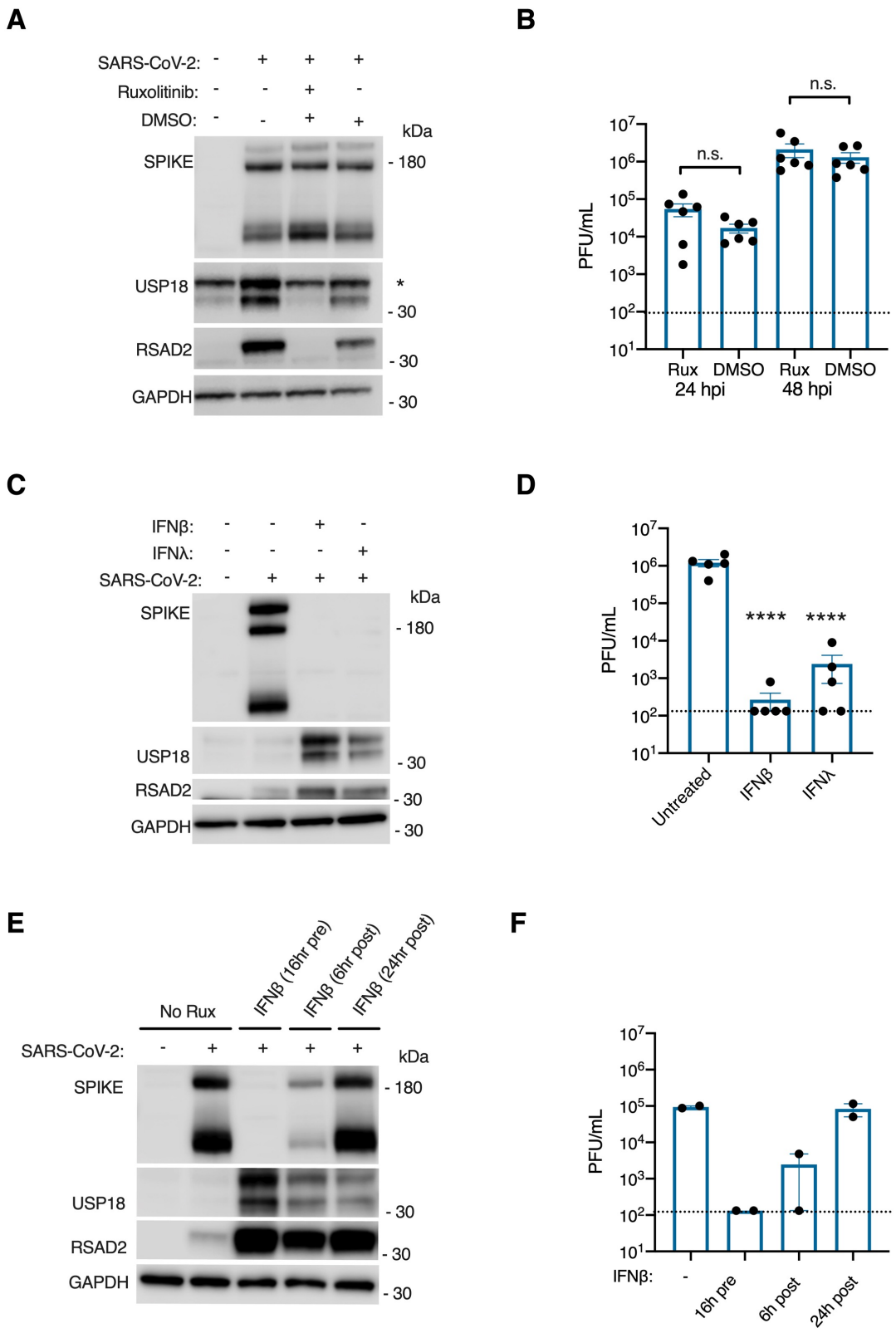

Figure 6. Impact IFN-I/III signalling on SARS-CoV-2 infection. (A) Immunoblot of nasal ALI cultures treated with ruxolitinib (RUX, 10 µM) or DMSO vehicle for 24 h prior to infection. Whole-cell lysates were prepared at 48 hpi. Results representative of experiments in n=4 donors (* = nonspecific band).

335 (B) Plaque assay showing no increase in infectious particle release at 24 hpi and 48 hpi (same
336 experimental conditions as A; n=6 donors). (C) Immunoblot of whole-cell lysates prepared from nasal
337 ALI cultures at 48 hpi (representative of n=4 donors). Cultures were pre-treated for 16 h prior to
338 infection with IFNβ (1000 IU/mL) or IFNλ1 (100 ng/mL). (D) Plaque assay showing significant reduction
339 in infectious particle release at 48 hpi if pre-treated with IFNβ (1000 IU/mL) or IFNλ1 (100 ng/mL)
340 (same experimental conditions as C; n=5 donors). (E) Immunoblot of whole-cell lysates prepared at 48
341 hpi. Nasal ALI cultures were either pre-treated with IFNβ (1000 IU/mL) for 16h prior to infection with
342 SARS-CoV-2 or IFNβ (1000 IU/mL) treatment was applied at 6 or 24 hpi. Results representative of
343 experiments in n=2 donors. (F) Plaque assay on supernatants collected from E (48 hpi). Mean ± SEM.
344 **** $P < 0.001$ n.s. = non-significant. ANOVA with Dunnett's post-test correction compared to vehicle
345 (B) or untreated control (F).

346 **DISCUSSION**

347 We report the most comprehensive characterisation of the human nasal epithelial response to SARS-
348 CoV-2 to date, revealing a response dominated by IFN-I/IIIs and their downstream ISG products. While
349 this is apparently insufficient to contain SARS-CoV-2, recombinant IFN-I/III treatment potently blocked
350 SARS-CoV-2 replication, suggesting that mucosal delivery of IFNs could be a promising strategy for
351 post-exposure prophylaxis.

352 The nasal mucosa is likely to be a main point of entry of SARS-CoV-2. Prior single-cell transcriptomic
353 studies implied an abundance of target cells in the nasal mucosa and further suggested that they may
354 be poised to mount an antiviral response[9]. Yet few studies to date have characterised SARS-CoV-2
355 replication in primary human differentiated nasal cells[11-13], and ours is the first to analyse the host-
356 virus interaction comprehensively, at single-cell resolution. Our findings indicate that the host
357 response to SARS-CoV-2 in nasal epithelium is dominated by IFN-I/III, albeit this response is kinetically
358 delayed. These results are consistent with evidence of IFN-I/III induction in nasal swabs from patients
359 with COVID-19[33]. However, we found that blockade of the endogenous IFN response did not impact
360 on SARS-CoV-2 infection. At first glance, this result may appear paradoxical. However, the probable
361 explanation is the delay of induction of IFN-I/III relative to virus replication. IFN-I/III expression
362 became detectable 36-48 h after the onset of SARS-CoV-2 replication - at a point at which infectious
363 virion production was reaching its maximum, and over half of cells in the culture were already infected
364 - suggesting the production of IFNs was too late to have a meaningful impact on the overall spread of
365 infection. Consistent with this, there was evidence of downregulation of PRR signalling in the
366 proteome of infected cells. We conclude that: (i) SARS-CoV-2 appears capable of evading PRR
367 signalling in nasal epithelial cells in the early stages of viral replication; and (ii) the endogenous IFN-
368 I/III response of nasal epithelial cells comes effectively "too little, too late" to inhibit SARS-CoV-2 in
369 the nasal epithelium. The expression of various IFN evasion proteins[34] and the sequestration of viral
370 replication machinery within cytosolic vesicles[35] underlie the capacity of SARS-CoV-2 to evade early
371 detection by PRRs, as indicated by our proteomics data. However, an important question is what

372 molecular patterns are responsible for IFN-I/III induction at later times. Future studies should address
373 the relative contribution of host damage-associated molecular patterns versus viral pathogen-
374 associated molecular patterns (e.g. defective viral genomes) accumulating during replication.
375 Our finding that exogenous IFN-I or IFN-III can potently induce an antiviral state in nasal cells is
376 consistent with its apparent protective effects in patients[16-18] and in early phase clinical trials[32]. The
377 main limitation of our data in this nasal epithelial culture system is that it did not account for
378 professional immune cells present in the nasal mucosa, for example plasmacytoid dendritic cells[36],
379 which are capable of more rapidly mounting an IFN-I/III response to SARS-CoV-2[37], potentially tipping
380 the scales in favour of the host. We studied cells derived from adult donors, however it is possible that
381 nasal cells from paediatric donors may behave differently in terms of their permissiveness to SARS-
382 CoV-2 and/or the efficiency of their innate immune response. Furthermore, SARS-CoV-2 variants with
383 mutations in the spike gene have emerged worldwide whilst we were undertaking the experiments
384 described here; these variants may impact viral replication and/or host immunity, and should be
385 included in future studies.
386 Nevertheless, our data, employing a variety of complementary methods, indicate that SARS-CoV-2 has
387 a relatively broad tropism for nasal epithelial cells, confirming suggestions from prior scRNA-seq
388 studies[7,9] and other *in vitro* studies of primary nasal[13] and tracheobronchial cells[22]. These findings
389 contrast with the results of Hou and colleagues, who reported exclusive tropism of SARS-CoV-2 for
390 ciliated cells in the airway[12]. It is not immediately clear how to reconcile these findings, given that
391 secretory cells express relevant entry receptors[12]. Hou and colleagues used a fluorescent reporter
392 virus, the tropism of which might have been slightly narrower than clinical isolates. It is also worth
393 noting our findings show that while all cell types contained SARS-CoV-2 protein, the intensity of
394 immunodetection was greater in ciliated cells, which also contained more virion-like structures per
395 cell. This implies that although all cell types are permissive, there may also be quantitative differences
396 in the efficiency of viral replication in different cell types. Hou and colleagues previously hypothesised
397 that post-entry factors such as antiviral immunity might dictate permissiveness. We found no evidence

398 to support this hypothesis, since while all nasal epithelial cells demonstrated a basal ISG signature -
399 consistent with *ex vivo* nasal biopsy data[9] - this did not vary substantially between cell types, and was
400 apparently insufficient to mediate resistance to SARS-CoV-2.
401 The observation that IFN-I treatment prevents SARS-CoV-2 infection indicates that chemoprophylaxis
402 with IFN-I may have therapeutic value. This approach has already been tested in a small clinical trial
403 in China (although the absence of a control group makes it impossible to judge the efficacy of this
404 approach[38]). Immunisation is the most tractable approach for large-scale primary prevention of
405 COVID-19. However, owing to incomplete vaccine coverage and/or effectiveness against mildly
406 symptomatic or asymptomatic infection, and the emergence of variants that may compromise vaccine
407 efficacy, there will likely continue to be a need for targeted chemoprophylactic therapies to prevent
408 transmission in specific circumstances. These include post-exposure prophylaxis of contacts - to avoid
409 the need for self-isolation - as well as pre-exposure prophylaxis for certain high-risk encounters (e.g.
410 in healthcare settings or prior to long-distance travel). Our data suggest that application of IFNβ to
411 the nasal mucosa might have an important role to play in this setting and argue for urgent clinical
412 assessment of this approach. In terms of the therapeutic efficacy of IFNβ in patients with COVID-19,
413 our findings suggest that early administration will likely be a key factor determining its efficacy.
414
415 **METHODS**
416 **Adult nasal airway epithelial cell culture at air-liquid interface (ALI)**
417 Adult primary human nasal airway epithelial cells were derived from excess clinical material obtained
418 during routine nasal surgical procedures, processed, differentiated and validated as previously
419 described[27] with the following modifications: cells were cryopreserved following expansion, then re-
420 animated and differentiated at ALI in PneumaCult-ALI-S (Stemcell Technologies). The sex and age of
421 donors are included in Table S3. Ethical approval for sample collection was provided (Research Ethics
422 Committee Reference 17/NE/0361).
423

424 **Viruses, cytokines and inhibitors**

425 A clinical isolate of SARS-CoV-2 (England/2/2020) was obtained from Public Health England (PHE). The
426 initial stock was propagated once in Vero E6 cells. The same viral stock was used for all experiments.
427 Sendai virus (Cantell Strain) was obtained from Richard Randall (St Andrew's University). For nasal ALI
428 infections, apical poles were gently washed once with warm Dulbecco's modified Eagle's medium
429 (DMEM; Gibco, USA) and then infected with 60 µL dilution of virus in DMEM, at a MOI of between 2
430 and 0.01 plaque-forming units per cell for 2 hours, when the virus-containing medium was removed.
431 DMEM was used as inoculum for mock infection. Apical washes (in warm phosphate-buffered saline)
432 were collected at different time-points and stored at -80°C for plaque assays. Plaque assays were
433 undertaken in Vero E6 cells using a 1.2% (w/v) microcrystalline cellulose overlay (Sigma-Aldrich).
434 Cytokines/inhibitors were used at the following concentrations: human recombinant IFNβ1 (1000
435 ng/mL; Avonex, Biogen Inc, USA); IFNλ1 (100 ng/mL; R&D Systems, USA); and Ruxolitinib (10 µM;
436 Calbiochem, USA) alongside the appropriate dilution of DMSO vehicle. Treatment was applied through
437 basolateral poles.

438

439 **Single cell RNA sequencing (scRNA-seq)**

440 For droplet-encapsulation cells were processed as described in the supplementary information (SI).
441 Principal component (PC) analysis was undertaken to find the first 20 PCs, which were batch-
442 adjusted using Harmony and used to generate the nearest-neighbour graph. Dimensionality
443 reduction and embedding was performed using Uniform Manifold Approximation and Projection
444 (UMAP), with the neighbourhood graph clustered using the Leiden algorithm. The Wilcoxon Rank
445 Sum test was used to identify differentially expressed genes between clusters, and these were
446 annotated based on expression of markers used in the literature to define populations. A published
447 gene set was used to generate a list of type I ISGs (www.gsea-
448 msigdb.org/gsea/msigdb/cards/GO_RESPONSE_TO_TYPE_I_INTERFERON). This was used to quantify
449 the interferon response within identified cell populations using the AddModuleScore tool in Seurat.

450 Infected cells were assigned as those cells with detectable SARS-CoV-2 spike RNA ('covid—S'
451 transcript). Further details are included in the SI.
452
453 **Proteome sample preparation**
454 The protein concentration was determined by EZQ® protein quantification assay. Protein digestion was
455 performed using the S-Trap™ sample preparation method and TMT-16 plex labelling was carried out
456 as per the manufacturer's instructions. Samples were cleaned using MacroSpin columns, and dried
457 down prior to offline high performance liquid chromatography fractionation. Peptides were
458 fractionated on a Basic Reverse Phase column on a Dionex Ultimate 3000 off-line LC system. A total of
459 18 fractions were collected, and each fraction was acidified and dried. Peptides were dissolved in 5%
460 formic acid, and each sample was independently analysed on an Orbitrap Fusion Lumos Tribrid mass
461 spectrometer, connected to an UltiMate 3000 RSLCnano System. All spectra were analysed using
462 MaxQuant 1.6.10.43 and searched against SwissProt *Homo sapiens* and Trembl SARS-CoV-2 FASTA
463 files. Reporter ion MS3 was used for quantification and the additional parameter of quantitation labels
464 with 16 plex TMT on N-terminus or lysine was included. A protein and peptide false discovery rate
465 (FDR) of less than 1% was employed in MaxQuant. Moderated *t*-tests, with patient accounted for in
466 the linear model, was performed using Limma, where proteins with an adjusted $P < 0.05$ were
467 considered as statistically significant. All analysis was performed using R. Raw data are present in
468 Supplementary Dataset 1. A comprehensive description of the methods can be found in the SI.
469
470 **Quantitative RT-PCR, immunoblotting and immunofluorescence**
471 RT-PCR and immunoblot were done as previously described[31], with further detail in the SI.
472 Membranes were fixed *in situ* with 4% formaldehyde overnight at 4°C, before sectioning.
473 Immunofluorescent staining was performed in accordance with published methods[39], with
474 modifications as summarised in the SI. Images were captured using a Nikon A1 confocal microscope

475 (Nikon, Japan) and analysed via Fiji (Version 2.0) using the Cell Counter plugin. Primers and probes
476 (Table S4) and antibodies (Table S5) are described in the SI.
477
478 **Transmission electron microscopy (TEM)**
479 ALI cultures were fixed with 2% glutaraldehyde (Sigma-Aldrich, MO, USA) with 0.1 M sodium
480 cacodylate (pH 7.4) buffer overnight at 4°C. TEM resin processing was performed as described
481 previously[40]. Additional details, including embedding, sectioning and analysis, are included in the SI.
482
483 **Statistical analysis**
484 Statistical analysis was performed and figures assembled using GraphPad Prism V8 (GraphPad
485 Software, USA). Data are presented as mean ± SEM of individual donor values (derived typically from
486 2-3 independent repeat experiments per donor). The donor was used as the unit of experiment for
487 statistical analysis purposes. Continuous data were normalised or log-transformed prior to analysis
488 using parametric significance tests. Differences between two groups were compared using an
489 unpaired, two-tailed Student's *t*-test, whereas differences between more than two groups used
490 ANOVA, with Dunnett's post-test correction for multiple comparisons. A two-tailed alpha of < 0.05
491 was the threshold for statistical significance. Statistical analysis of proteomics and transcriptomics
492 data sets is described in the relevant sections above.
493
494 **Data availability**
495 The mass spectrometry proteomics data have been deposited to the ProteomeXchange Consortium[41]
496 via the PRIDE partner repository[42] with the dataset identifier PXD021026. Reviewers can access it
497 through the Username: reviewer_pxd022523@ebi.ac.uk and the Password: UaEXYFKF. RNA
498 sequencing data have been deposited to the European Genome-phenome archive (accession
499 pending). Additional raw data are available on request from the corresponding author.
500

Acknowledgements

We acknowledge Public Health England for providing the SARS-CoV-2 isolate and Professor R Randall (St Andrew's University) for providing Sendai virus and the Vero E6 cell line. We thank A Khan, M Glanville and S Dainty (Newcastle University Infectious Disease Facility) and A Laude (Bioimaging facility) for assistance. The work was part-funded by the Barbour Foundation (CJAD, SH, MB, MT, MH, CW), the UK-Coronavirus Immunology Consortium (CJAD, SH, MH) and the Medical Research Council SHIELD antimicrobial resistance consortium (JS, AJS). CFH is supported by a Medical Research Council studentship (MR/NO13840/1) and MB by an MRC Clinician Scientist Fellowship (MR/M008797/1). MT and SH are funded by a Wellcome Trust Investigator Awards (215542/Z/19/Z and 207556/Z/17/Z). CJAD and GR are Wellcome Trust Clinical Research Career Development Fellows (211153/Z/18/Z and 214539/Z/18/Z). MED is a Marie Sklodowska Curie Fellow within the European Union's Horizon 2020 research and innovation programme under the Marie Sklodowska-Curie grant agreement No. 890296. MH is funded by Wellcome (WT107931/Z/15/Z), The Lister Institute for Preventive Medicine and Newcastle NIHR Biomedical Research Centre (BRC). JPG, CW and BV were supported by the Medical Research Foundation (MRF Respiratory Diseases Research Award to JPG; Grant MRF-091-0001-RGGARNE) and Boehringer Ingelheim. TEM work was supported by a BBSRC Alert17 grant (BB/R013942/1). Professor Simpson is a National Institute for Health Research (NIHR) Senior Investigator. The views expressed in this article are those of the author(s) and not necessarily those of the NIHR, or the Department of Health and Social Care.

Author contributions

Conceived the study: MB, CW, CJAD with MH, SH, MT. Experimental design: MH, SH, MB, CW, MT, GR, CJAD. Nasal model development and patient material: IJH, BV, JS, JPG, SC, AJS, MB, CW. Virology data generation, analysis and interpretation: CFH, BJT, JSS, FG, AIG, TD, SH, CJAD. Proteomics data generation, analysis and interpretation: MED, SM, MT. Single-cell sequencing data generation, analysis and interpretation: RAB, ES, RH, JC, MH, GR. Supervised research: AJS, MH, SH, MB, CW, MT,

GR, CJAD. Drafted the manuscript: CFH and CJAD with ES, BV, MED, TD, MT, GR. Revised the manuscript: RAB, MED, IJH, JSS, AJS, MH, SH, CW. Approved the manuscript for submission: all authors.

530 **References**

531 1 Zhu, N. *et al.* A Novel Coronavirus from Patients with Pneumonia in China, 2019. *N Engl J Med*
532 **382**, 727-733, doi:10.1056/NEJMoa2001017 (2020).
533 2 Hoffmann, M. *et al.* SARS-CoV-2 Cell Entry Depends on ACE2 and TMPRSS2 and Is Blocked by
534 a Clinically Proven Protease Inhibitor. *Cell* **181**, 271-280 e278, doi:10.1016/j.cell.2020.02.052
535 (2020).
536 3 Huang, C. *et al.* Clinical features of patients infected with 2019 novel coronavirus in Wuhan,
537 China. *Lancet* **395**, 497-506, doi:10.1016/S0140-6736(20)30183-5 (2020).
538 4 Knight, S. R. *et al.* Risk stratification of patients admitted to hospital with covid-19 using the
539 ISARIC WHO Clinical Characterisation Protocol: development and validation of the 4C
540 Mortality Score. *BMJ* **370**, m3339, doi:10.1136/bmj.m3339 (2020).
541 5 Group, R. C. *et al.* Dexamethasone in Hospitalized Patients with Covid-19 - Preliminary Report.
542 *N Engl J Med*, doi:10.1056/NEJMoa2021436 (2020).
543 6 Cevik, M., Kuppalli, K., Kindrachuk, J. & Peiris, M. Virology, transmission, and pathogenesis of
544 SARS-CoV-2. *BMJ* **371**, m3862, doi:10.1136/bmj.m3862 (2020).
545 7 Chen, M. *et al.* Elevated ACE-2 expression in the olfactory neuroepithelium: implications for
546 anosmia and upper respiratory SARS-CoV-2 entry and replication. *Eur Respir J* **56**,
547 doi:10.1183/13993003.01948-2020 (2020).
548 8 Hoagland, D. A. *et al.* Leveraging the antiviral type I interferon system as a first line of defense
549 against SARS-CoV-2 pathogenicity. *Immunity*, doi:10.1016/j.immuni.2021.01.017 (2021).
550 9 Sungnak, W. *et al.* SARS-CoV-2 entry factors are highly expressed in nasal epithelial cells
551 together with innate immune genes. *Nat Med* **26**, 681-687, doi:10.1038/s41591-020-0868-6
552 (2020).
553 10 Ziegler, C. G. K. *et al.* SARS-CoV-2 Receptor ACE2 Is an Interferon-Stimulated Gene in Human
554 Airway Epithelial Cells and Is Detected in Specific Cell Subsets across Tissues. *Cell* **181**, 1016-
555 1035 e1019, doi:10.1016/j.cell.2020.04.035 (2020).
556 11 Gamage, A. M. *et al.* Infection of human Nasal Epithelial Cells with SARS-CoV-2 and a 382-nt
557 deletion isolate lacking ORF8 reveals similar viral kinetics and host transcriptional profiles.
558 *PLoS Pathog* **16**, e1009130, doi:10.1371/journal.ppat.1009130 (2020).
559 12 Hou, Y. J. *et al.* SARS-CoV-2 Reverse Genetics Reveals a Variable Infection Gradient in the
560 Respiratory Tract. *Cell* **182**, 429-446 e414, doi:10.1016/j.cell.2020.05.042 (2020).
561 13 Pizzorno, A. *et al.* Characterization and Treatment of SARS-CoV-2 in Nasal and Bronchial
562 Human Airway Epithelia. *Cell Rep Med* **1**, 100059, doi:10.1016/j.xcrm.2020.100059 (2020).
563 14 Onabajo, O. O. *et al.* Interferons and viruses induce a novel truncated ACE2 isoform and not
564 the full-length SARS-CoV-2 receptor. *Nat Genet* **52**, 1283-1293, doi:10.1038/s41588-020-
565 00731-9 (2020).
566 15 Duncan, C. J. A., Randall, R. E. & Hambleton, S. Genetic Lesions of Type I Interferon Signalling
567 in Human Antiviral Immunity. *Trends Genet* **37**, 46-58, doi:10.1016/j.tig.2020.08.017 (2021).
568 16 Zhang, Q. *et al.* Inborn errors of type I IFN immunity in patients with life-threatening COVID-
569 19. *Science* **370**, doi:10.1126/science.abd4570 (2020).
570 17 Pairo-Castineira, E. *et al.* Genetic mechanisms of critical illness in Covid-19. *Nature*,
571 doi:10.1038/s41586-020-03065-y (2020).
572 18 Bastard, P. *et al.* Autoantibodies against type I IFNs in patients with life-threatening COVID-
573 19. *Science* **370**, doi:10.1126/science.abd4585 (2020).
574 19 Lokugamage, K. G. *et al.* Type I Interferon Susceptibility Distinguishes SARS-CoV-2 from SARS-
575 CoV. *J Virol* **94**, doi:10.1128/JVI.01410-20 (2020).
576 20 Felgenhauer, U. *et al.* Inhibition of SARS-CoV-2 by type I and type III interferons. *J Biol Chem*
577 **295**, 13958-13964, doi:10.1074/jbc.AC120.013788 (2020).
578 21 Lee, J. S. & Shin, E. C. The type I interferon response in COVID-19: implications for treatment.
579 *Nat Rev Immunol* **20**, 585-586, doi:10.1038/s41577-020-00429-3 (2020).

580 22 Zhu, N. *et al.* Morphogenesis and cytopathic effect of SARS-CoV-2 infection in human airway
581 epithelial cells. *Nat Commun* **11**, 3910, doi:10.1038/s41467-020-17796-z (2020).
582 23 Fiege, J. K. *et al.* Single cell resolution of SARS-CoV-2 tropism, antiviral responses, and
583 susceptibility to therapies in primary human airway epithelium. *PLoS Pathog* **17**, e1009292,
584 doi:10.1371/journal.ppat.1009292 (2021).
585 24 Vanderheiden, A. *et al.* Type I and Type III Interferons Restrict SARS-CoV-2 Infection of Human
586 Airway Epithelial Cultures. *J Virol* **94**, doi:10.1128/JVI.00985-20 (2020).
587 25 Blanco-Melo, D. *et al.* Imbalanced Host Response to SARS-CoV-2 Drives Development of
588 COVID-19. *Cell* **181**, 1036-1045 e1039, doi:10.1016/j.cell.2020.04.026 (2020).
589 26 Huang, J. *et al.* SARS-CoV-2 Infection of Pluripotent Stem Cell-derived Human Lung Alveolar
590 Type 2 Cells Elicits a Rapid Epithelial-Intrinsic Inflammatory Response. *bioRxiv*,
591 doi:10.1101/2020.06.30.175695 (2020).
592 27 Mavin, E. *et al.* Real-time measurement of cellular bioenergetics in fully differentiated human
593 nasal epithelial cells grown at air-liquid-interface. *Am J Physiol Lung Cell Mol Physiol* **318**,
594 L1158-L1164, doi:10.1152/ajplung.00414.2019 (2020).
595 28 Xiu, S. *et al.* Inhibitors of SARS-CoV-2 Entry: Current and Future Opportunities. *J Med Chem*
596 **63**, 12256-12274, doi:10.1021/acs.jmedchem.0c00502 (2020).
597 29 Randall, R. E. & Goodbourn, S. Interferons and viruses: an interplay between induction,
598 signalling, antiviral responses and virus countermeasures. *J Gen Virol* **89**, 1-47,
599 doi:10.1099/vir.0.83391-0 (2008).
600 30 Wu, X. *et al.* Intrinsic Immunity Shapes Viral Resistance of Stem Cells. *Cell* **172**, 423-438 e425,
601 doi:10.1016/j.cell.2017.11.018 (2018).
602 31 Duncan, C. J. A. *et al.* Severe type I interferonopathy and unrestrained interferon signaling due
603 to a homozygous germline mutation in STAT2. *Sci Immunol* **4**,
604 doi:10.1126/sciimmunol.aav7501 (2019).
605 32 Monk, P. D. *et al.* Safety and efficacy of inhaled nebulised interferon beta-1a (SNG001) for
606 treatment of SARS-CoV-2 infection: a randomised, double-blind, placebo-controlled, phase 2
607 trial. *Lancet Respir Med*, doi:10.1016/S2213-2600(20)30511-7 (2020).
608 33 Antonelli, G. *et al.* Type I interferons can be detected in respiratory swabs from SARS-Cov-2
609 infected patients. *J Clin Virol* **128**, 104450, doi:10.1016/j.jcv.2020.104450 (2020).
610 34 Lei, X. *et al.* Activation and evasion of type I interferon responses by SARS-CoV-2. *Nat Commun*
611 **11**, 3810, doi:10.1038/s41467-020-17665-9 (2020).
612 35 Wolff, G., Melia, C. E., Snijder, E. J. & Barcena, M. Double-Membrane Vesicles as Platforms for
613 Viral Replication. *Trends Microbiol* **28**, 1022-1033, doi:10.1016/j.tim.2020.05.009 (2020).
614 36 Hartmann, E. *et al.* Analysis of plasmacytoid and myeloid dendritic cells in nasal epithelium.
615 *Clin Vaccine Immunol* **13**, 1278-1286, doi:10.1128/CVI.00172-06 (2006).
616 37 Onodi, F. *et al.* SARS-CoV-2 induces human plasmacytoid pre-dendritic cell diversification via
617 UNC93B and IRAK4. *bioRxiv*, doi:10.1101/2020.07.10.197343 (2021).
618 38 Meng, Z. *et al.* An experimental trial of recombinant human interferon alpha nasal drops to
619 prevent COVID-19 in medical staff in an epidemic area. *MedRxiv*,
620 doi:doi.org/10.1101/2020.04.11.20061473 (2020).
621 39 Crowe, A. R. & Yue, W. Semi-quantitative Determination of Protein Expression using
622 Immunohistochemistry Staining and Analysis: An Integrated Protocol. *Bio Protoc* **9**,
623 doi:10.21769/BioProtoc.3465 (2019).
624 40 Faitg, J., Davey, T., Turnbull, D. M., White, K. & Vincent, A. E. Mitochondrial morphology and
625 function: two for the price of one! *J Microsc* **278**, 89-106, doi:10.1111/jmi.12891 (2020).
626 41 Deutsch, E. W. *et al.* The ProteomeXchange consortium in 2017: supporting the cultural
627 change in proteomics public data deposition. *Nucleic Acids Res* **45**, D1100-D1106,
628 doi:10.1093/nar/gkw936 (2017).

42 Perez-Riverol, Y. *et al.* The PRIDE database and related tools and resources in 2019: improving support for quantification data. *Nucleic Acids Res* **47**, D442-D450, doi:10.1093/nar/gky1106 (2019).